Interactions of Aqueous NOM with Nanoscale TiO2: Implications for Ceramic Membrane Filtration−Ozonation Hybrid Process

ARTICLE *in* ENVIRONMENTAL SCIENCE AND TECHNOLOGY · AUGUST 2009

Impact Factor: 5.33 · DOI: 10.1021/es900342q · Source: PubMed

6 AUTHORS, INCLUDING:

Wenqian Shan
Michigan State University
10 PUBLICATIONS **359** CITATIONS
SEE PROFILE

Melissa J Baumann
Auburn University
47 PUBLICATIONS **957** CITATIONS
SEE PROFILE

Susan J Masten
Michigan State University
79 PUBLICATIONS **1,709** CITATIONS
SEE PROFILE

Vlad Tarabara
Michigan State University
63 PUBLICATIONS **950** CITATIONS
SEE PROFILE

Environ. Sci. Technol. **2009,** *43,* 5488–5494

Interactions of Aqueous NOM with Nanoscale TiO_2: Implications for Ceramic Membrane Filtration-Ozonation Hybrid Process

JEONGHWAN KIM,[†,‡] WENQIAN SHAN,[†] SIMON H. R. DAVIES,[†] MELISSA J. BAUMANN,[§] SUSAN J. MASTEN,[†] AND VOLODYMYR V. TARABARA*,[†]

Department of Civil and Environmental Engineering, Michigan State University, East Lansing, Michigan 48823, Department of Environmental Engineering, INHA University, 253 Yonghyun-dong, Nam-gu, Incheon, 402-751, Republic of Korea, and Department of Chemical Engineering and Materials Science, Michigan State University, East Lansing, Michigan 48823

Received February 3, 2009. Revised manuscript received May 4, 2009. Accepted May 12, 2009.

The combined effect of pH and calcium on the interactions of nonozonated and ozonated natural organic matter (NOM) with nanoscale TiO_2 was investigated. The approach included characterization of TiO_2 nanoparticles and NOM, extended Derjaguin–Landau–Verwey–Overbeek (XDLVO) modeling of NOM-TiO_2 and NOM–NOM interactions, batch study on the NOM adsorption onto TiO_2 surface, and bench-scale study on the treatment of NOM-containing feed waters using a hybrid process that combines ozonation and ultrafiltration with a 5 kDa ceramic (TiO_2 surface) membrane. It was demonstrated that depending on pH and TiO_2 loading, the adsorption of NOM species is controlled by either the availability of divalent cations or by preozonation of NOM. XDLVO surface energy analysis predicts NOM adsorption onto TiO_2 in the ozone-controlled regime but not in the calcium-controlled regime. In both regimes, short-range NOM–NOM and NOM–TiO_2 interactions were governed by acid–base and van der Waals forces, whereas the role of electrostatic forces was relatively insignificant. Ozonation increased the surface energy of NOM, contributing to the hydrophilic repulsion component of the NOM–NOM and NOM–TiO_2 interactions. In the calcium-controlled regime, neither NOM–TiO_2 nor NOM–NOM interaction controlled adsorption. Non-XDLVO interactions such as intermolecular bridging by calcium were hypothesized to be responsible for the observed adsorption behavior. Adsorption data proved to be highly predictive of the permeate flux performance.

1. Introduction

Nanoscale TiO_2 is widely used in ceramic membrane manufacturing. TiO_2 has also been used to fabricate nano-composite membranes (*1*–*4*) and as a catalyst in advanced oxidation processes (*5*–*12*). The performance of catalytic and membrane processes can be compromised by fouling of the catalyst and the membrane surface (*12*). Specifically, with the treatment of natural waters, NOM fouling is a long-standing problem (*13, 14*). NOM is known to adsorb at the solid surfaces (e.g., membranes, colloids) in water and modify their properties including charge and hydrophilicity (*13, 15*–*17*). As with polymeric membrane fouling (*18*–*21*), NOM fouling of ceramic membranes can be expected to be governed by the NOM-membrane interactions (*22*). NOM is also of concern in water treatment systems as it reacts with chlorine, the most commonly used disinfectant in the U.S., to form carcinogenic chlorinated compounds.

The combination of an advanced oxidation process and membrane separation—hybrid ozone-membrane filtration—has been shown to have significant potential in mitigating both the NOM fouling of membranes and the formation of disinfection byproducts (*5*–*8, 12, 23, 24*). The mitigating effect is due, in part, to the ability of ozone to effectively and preferentially oxidize electron-rich moieties and carbon–carbon double bonds of organic molecules. The catalytic activity of the TiO_2 nanoparticles, components of the membrane structure in the hybrid system, to further enhance the high reactivity of ozone with NOM (*25*) and to mitigate NOM fouling. Ceramic membranes, which are ozone-resistant, can be used with ozone to achieve high permeate flux without membrane damage (*5, 6, 8, 12, 23*). Our previous studies (*5*–*7, 12*) have shown that the hybrid ozonation-UF ceramic membrane process can reduce membrane fouling. While the results of these studies are encouraging, there remains a need to better understand fouling mechanisms and how the system behaves over a wide range of chemical conditions.

The objective of this work was to investigate the combined effect of pH and divalent ions such as calcium on the interactions of NOM (both nonozonated and ozonated) with nanoscale TiO_2. The approach was four-tiered and included (i) experimental characterization of TiO_2 nanoparticles and (ozonated and nonozonated) NOM, (ii) XDLVO modeling of NOM-TiO_2 interactions, (iii) batch studies on the NOM adsorption onto TiO_2 surface, and (iv) bench-scale filtration studies with synthetic NOM-containing feed waters using a hybrid ozonation-ultrafiltration system. The predictive capability and interpretive value of XDLVO modeling for the understanding of NOM sorption onto nanoscale TiO_2 was evaluated. The performance of the hybrid ozonation-filtration process was compared to the predictions of the XDLVO model and the batch adsorption experimental data to elucidate the most important physicochemical phenomena that influence permeate flux behavior.

2. Experimental Section

2.1. TiO_2 Nanoparticles and NOM. TiO_2 particles (TiO_2 nanopowder, <100 nm (BET), mixture of rutile and anatase, 99.9% metals basis, Aldrich) were used as received. Suwannee River NOM (SRNOM), isolated by reverse osmosis, was purchased from International Humic Substances Society (Denver, CO). A 20 mg/L suspension of SRNOM was prepared by dispersing the SRNOM in deionized (DI) water. The total organic carbon (TOC) content of the SRNOM feed solution was 10 ± 0.5 mg C/L. The pH of the solution was adjusted by adding either HCl or NaOH and a borate (0.0625 mmol/L) buffer solution. The borate buffer was prepared by mixing aqueous solutions of $Na_2B_4O_7 \cdot 10H_2O$ (100 mL, 0.025 M) and HCl (41 mL, 0.1 M). Prior to each filtration experiment,

* Corresponding author phone: (517) 432-1755; fax: (517) 355-0250; e-mail: tarabara@msu.edu.
† Department of Civil and Environmental Engineering, Michigan State University.
‡ INHA University.
§ Department of Chemical Engineering and Materials Science, Michigan State University.

10.1021/es900342q CCC: $40.75

Published on Web 06/16/2009

the ionic strength of the solution was adjusted to 7.5 × 10^{-3} M using 10^{-2} M NaCl.

2.2. Surface Charge Measurements. A 20 mg/L suspension of SRNOM and a 0.5 g/L suspension of TiO_2 particles were prepared for the zeta potential measurements. The electrophoretic mobility was measured by phase analysis light scattering (ZetaPALS, Brookhaven Instrument Corp., Holtsville, NY) and converted into zeta potential using the Smoluchowski equation. Acidimetric-alkalimetric titrations were performed to estimate the number of adsorption sites on the TiO_2 surface (*26*), (see the Supporting Information (SI)).

2.3. Contact Angle Measurements. The TiO_2, nonozonated SRNOM and ozonated SRNOM suspensions were filtered through 1 kDa polyethersulfone UF membranes (Pall Corp., East Hills, NY) using a stainless steel filtration cell (HP4750, Sterlitech Corp., Kent, WA) without stirring. Prior to the filtration, membranes were soaked in DI water for at least 10 h at room temperature and 200 mL of DI water was filtered through each membrane to remove trace chemicals, as recommended by the manufacturer. The ionic strength, pH, Ca^{2+} concentration of all the suspensions (see SI Table SI1) were adjusted prior to filtration. The SEM micrographs (SI Figure SI1) show that the material deposited on the membrane surface formed a cake layer, ca. 0.2 μm thick. For the ozonated SRNOM solutions with and without Ca^{2+}, the first 600 mL were filtered twice to improve NOM recovery. The membranes with deposits were dried in a desiccator before the contact angles were measured. The contact angles for three materials (TiO_2, ozonated SRNOM, and nonozonated SRNOM) were determined at three different pH values (3, 5, and 8) and two concentrations of Ca^{2+} (0 mM, 1 mM). Thus, contact angles were measured for a total of 18 different material/solution chemistry combinations.

A FTÅ 200 analyzer (First Ten Ångstroms, Portsmouth, VA) was used to measure contact angles. Measurements were carried out with three different probe liquids: aqueous solution, glycerol (Columbus Chemical Industries, Inc., Columbus WI), and diiodomethane (Spectrum Quality Products Inc., Gardena, CA). The ionic strength, pH, and calcium concentration of the DI water were adjusted to match the water chemistry in the droplet to that of the suspensions from which the TiO_2 and SRNOM deposits on membrane filters were formed. Measurements were made by forming, at the rate of 0.5 μL/s, a 5 μL drop of liquid on the tip of a stainless steel syringe needle and then placing the drop onto the membrane surface by raising the membrane until contact was made. An image of the drop was taken 2 s after the formation of the droplet and the left and the right contact angles were measured. For each probe liquid-sample combination at least two membrane coupons were analyzed with five images recorded for each membrane coupon.

2.4. Determination of Surface Tension Energies. The XDLVO theory predicts the energy of particle−particle and particle−surface interaction (*27*−*29*). The XDLVO model has been applied to describe how aqueous colloids interact with surfaces of polymeric membranes (*30*−*32*). Besides gravity and hydrodynamic forces, particles also experience noncovalent forces that include van der Waals force (F_{LW}), electrostatic double layer force (F_{EL}), and Lewis acid−base force (F_{AB}). XDLVO is an extended DLVO model wherein acid−base (polar) interactions are also taken into consideration (*33*). Incorporation of the polar interactions has been shown to result in a significant change in the predicted energies of *short-range* (<5 nm) colloid−colloid and colloid-surface interactions.

In this work we determine the interaction energy (free energy of adhesion) per unit area between *two planar surfaces with surface tension parameters and charges of NOM and TiO_2*. Although the model does not take into the account the size distribution of NOM molecules and the likely differences in hydrophilicity and charge between various size fractions of NOM, this approach should adequately describe effects, averaged over all NOM sizes, of ozonation-, pH-, and calcium-induced changes in NOM chemistry on the NOM-TiO_2 interactions.

The free energy of adhesion per unit area between two planar surfaces due to van der Waals forces is calculated as follows (*33*):

$$\Delta G_{y_0}^{LW} = 2\left(\sqrt{\gamma_w^{LW}} - \sqrt{\gamma_m^{LW}}\right)\cdot\left(\sqrt{\gamma_c^{LW}} - \sqrt{\gamma_w^{LW}}\right) \quad (1)$$

where $\gamma_w{}^{LW}$, $\gamma_m{}^{LW}$, and $\gamma_c{}^{LW}$ are LW components of the surface tension for water, the membrane, and colloids, respectively. Here, $\Delta G_{y_0}^{LW}$ is the LW free energy of adhesion between a membrane and a colloid that are at a distance of y_0, which is the minimum equilibrium cutoff distance due to Born repulsion and is usually assigned a value of 0.157 nm (*33*). The free energy of adhesion per unit area between two planar surfaces due to EL (electrostatic) interaction can be estimated using the following expression (*34*):

$$\Delta G_{y_0}^{EL} = \varepsilon_0\varepsilon_r\cdot\psi_c\psi_m/\lambda_{EL}, \text{ where } \lambda_{EL} = (3.28\times 10^9\sqrt{C_{el}})^{-1} \quad (2)$$

where $\varepsilon_r\varepsilon_0$ is the dielectric permittivity of the bulk fluid; ψ_c and ψ_m are the surface potentials (approximated, in this work, by zeta potentials ζ_c and ζ_m) of the colloid and membrane, respectively; C_{el} is the concentration of the background electrolyte in mol/L; λ_{EL} is the characteristic decay length for EL interactions in water.

The free energy of adhesion per unit area between two planar surfaces due to acid−base (AB) interaction is given by

$$\Delta G_{y_0}^{AB} = 2\sqrt{\gamma_w^+}\left(\sqrt{\gamma_m^-} + \sqrt{\gamma_c^-} - \sqrt{\gamma_w^-}\right) + 2\sqrt{\gamma_w^-}\left(\sqrt{\gamma_m^+} + \sqrt{\gamma_c^+} - \sqrt{\gamma_w^+}\right) - 2\left(\sqrt{\gamma_m^+\gamma_c^-} + \sqrt{\gamma_m^-\gamma_c^+}\right) \quad (3)$$

where γ^+ and γ^- are, respectively, the electron acceptor and electron donor components of the free energy. The surface tension parameters of foulants ($\gamma_c{}^+$, $\gamma_c{}^-$, $\gamma_c{}^{AB}$, $\gamma_c{}^{LW}$, $\gamma_c{}^{TOT}$) and membranes ($\gamma_m{}^+$, $\gamma_m{}^-$, $\gamma_m{}^{AB}$, $\gamma_m{}^{LW}$, $\gamma_m{}^{TOT}$) can be determined from the extended Young equation after measuring contact angle data for three probe liquids with known surface tension parameters ($\gamma_l{}^{LW}$, $\gamma_l{}^+$, $\gamma_l{}^-$):

$$(1+\cos\theta)\gamma_l^{TOT} = 2\left(\sqrt{\gamma_s^{LW}\gamma_l^{LW}} + \sqrt{\gamma_s^+\gamma_l^-} + \sqrt{\gamma_s^-\gamma_l^+}\right) \quad (4)$$

$$\gamma^{AB} = 2\sqrt{\gamma^+\gamma^-} \quad (5)$$

$$\gamma^{TOT} = \gamma^{AB} + \gamma^{LW} \quad (6)$$

where θ is the contact angle for a given probe liquid. The subscripts *s* and *l* correspond to the solid surface and the liquid, respectively.

2.5. Adsorption Measurements. In the adsorption experiments, where appropriate, 0.05 M aqueous solution of $CaCl_2$ was added to achieve the total added calcium concentration of 10^{-3} M. The resulting feed solutions were used either as prepared or were ozonated at an applied dosage of ca. 4 mg($[O_3]_g$)/L·min.

To measure the kinetics of SRNOM sorption by the TiO_2 nanoparticles, Teflon-capped pyrex glass bottles were filled with ca. 100 mL of 20 mg/L SRNOM solutions. After 5 min of stirring, ca. 40 mL of the solution were collected and analyzed to determine the concentration of the dissolved SRNOM; this value was considered to represent the initial

liquid phase concentration of the adsorbate. Measured amounts of TiO_2 nanoparticles were then added into each bottle to bring the suspended solids content in the TiO_2 suspensions to 0.5 g/L. The bottles were then placed on a shaker and shaken at room temperature for 24 h. Samples of the suspension were periodically collected, filtered through a 0.22 μm mixed cellulose esters filter (Millipore Corp., Bedford, MA), and then centrifuged at ca. 7500 rpm for 20 min to remove NOM associated with residual TiO_2 particles that might have been present in the filtrate. The SRNOM concentration in the dissolved phase was measured using a TOC analyzer (OI Analytical model 1010 Analyzer, College Station, TX). The amount of adsorbed SRNOM was calculated as the difference between the initial concentration and the measured equilibrium concentration of SRNOM in each vial.

To measure the adsorption isotherms Teflon-capped pyrex glass bottles were filled with 50 mL of the feed solution and different amounts of the dry sorbent (TiO_2 particles). The bottles were then placed on a shaker and were shaken at room temperature for 24 h. After the equilibration period the suspensions were filtered through a 0.22 μm mixed cellulose ester filter (Millipore Corp., Bedford, MA) and centrifuged to remove the TiO_2 particles. The amount of adsorbed SRNOM was calculated as describe above.

2.6. Hybrid Ceramic Membrane Filtration-Ozonation Tests. The hybrid ultrafiltration-ozonation system used in this study has been described in detail elsewhere (*12*). The system is illustrated in SI Figure SI2. Briefly, the pressurized hybrid system was operated in a crossflow mode using a variable speed pump to circulate the retentate. To maintain the volume of the retentate at an approximately constant value (ca. 0.6 L), a conductivity level sensor was installed to control the solenoid valve that regulated the inflow of the feedwater from the feed tank. The temperature of the water was maintained at 20 ± 0.5 °C by circulating chilled water through a stainless-steel coil immersed in the feed tank. The permeate flow rate was determined by collecting the permeate in a beaker positioned on an electronic balance (Adventure Pro, Ohaus, U.S.) and continually recording the mass of the permeate.

A tubular ceramic UF membrane (Attaxx, U.S.) with a molecular weight cutoff of 5 kDa was used in all filtration experiments. The membrane had an inner diameter of 0.6 cm, a length of 25 cm, and a surface area of 15 cm^2. The membrane consisted of alumina (Al_2O_3) support and a titania (TiO_2, rutile) separation layer. The membrane was housed in a stainless steel filter holder (TAMI North America, St. Laurent, QC, Canada).

The ceramic UF membrane was operated at a constant transmembrane pressure of 20 psi (138 kPa) and a crossflow velocity of 0.47 m/s. The concentration of SRNOM was 20 mg/L and TOC of the SRNOM solution was ca. 10 mg/L. To investigate the effect of calcium, the calcium concentration was adjusted to 10^{-3} M by adding $CaCl_2$ (0.05 M solution) into the SRNOM solution.

Pure oxygen from a gas cylinder was dried using a moisture trap containing anhydrous calcium sulfate and then fed to an ozone generator (Ozone Solutions, AC-500). An ozone-compatible compressor (OZC-110, Ozone Solutions) was connected to the ozone generator to pressurize the ozone gas to ca. 30 kPa (4.4 psi) above the operating pressure of filtration system. The ozone gas flow rate (Q_g) and ozone concentration in the gas phase ($[O_3]_g$) were set at 200 mL/min and 9.5 g/m^3, respectively. The dissolved ozone concentration in the retentate was monitored using an amperometric ozone microsensor (AMT Analysenmesstechnik GmbH, Rostock, Germany) and the applied dose was estimated about 4.5 mg/L·min. In the membrane filtration experiments the hydraulic detention time of the system, in the absence of fouling, was approximately 30 min. Assuming this detention time, the ozone dosage applied during the adsorption test was the same as that applied in the hybrid ozone-membrane experiments.

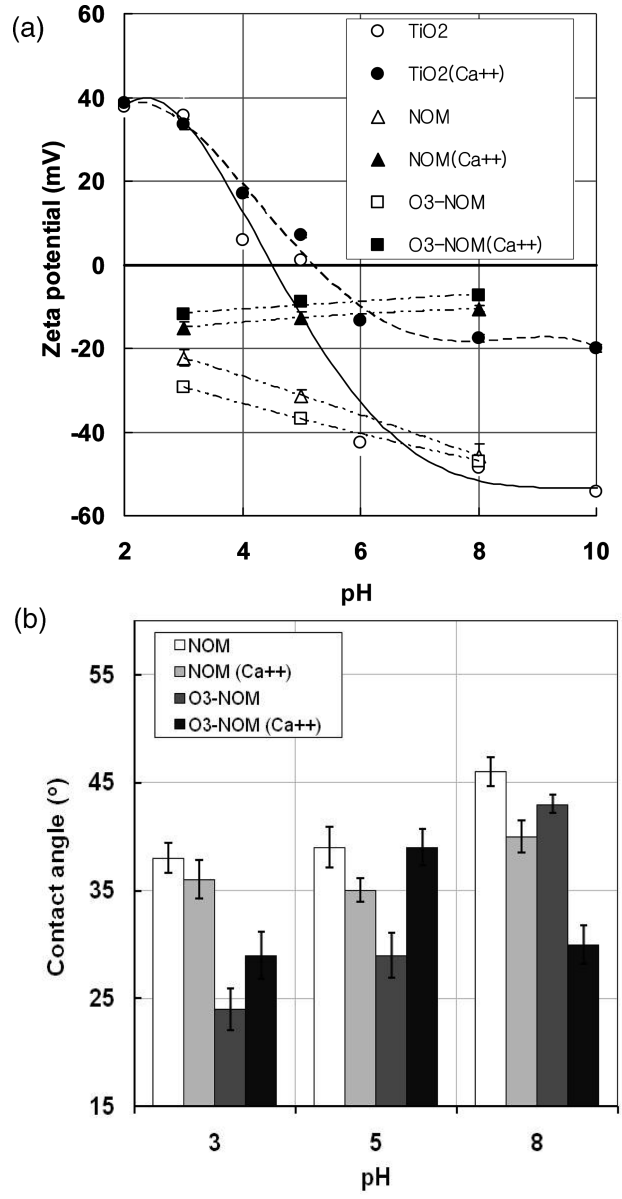

FIGURE 1. Combined effect of pH, Ca^{2+} and preozonation on (a) the zeta potential of TiO_2 nanoparticles and SRNOM, and (b) hydrophilicity of SRNOM. The error bars correspond to 90% confidence intervals.

3. Results and Discussion

3.1. Surface Charge of TiO_2 Nanoparticles and SRNOM. The pH dependence of the zeta potential of TiO_2 nanoparticles indicates an isoelectric point of ca. 4.5 (Figure 1a). At pH values greater than the isoelectric point, Ca^{2+} may adsorb onto TiO_2 nanoparticles, which will increase the surface charge (*35*). At pH values significantly less than the isoelectric point, Ca^{2+} is not sorbed due to the electrostatic repulsion between calcium cations and the positively charged TiO_2 surface. These results are consistent with results reported for metal (Al, Si, Mn, Fe) oxide nanoparticles and ozonated SRNOM (*36*). In the absence of Ca^{2+}, the zeta potential of SRNOM and ozonated SRNOM decreased with an increase in pH due to the deprotonation of carboxylic groups of SRNOM at higher pH. To the contrary, in the presence of Ca^{2+} a slight increase in the zeta potential of ozonated and

nonozonated SRNOM with pH was observed. This behavior suggests that increased binding of Ca^{2+} occurs at higher pH due to the complexation of Ca^{2+} by carboxylate sites on the NOM (*37*). While the ζ(pH) trend for the ozonated and nonozonated SRNOM was the same, the effect of calcium was more pronounced for ozonated SRNOM (-■- vs -□-, Figure 1a) than for nonozonated SRNOM (-▲-vs -Δ-, Figure 1a). This is consistent with the observation that the ozonation of aqueous NOM increases the contents of hydroxyl, carbonyl, and carboxyl functional groups (*36, 38*) that can form complexes with calcium.

3.2. Hydrophilicity of SRNOM. Figure 1b illustrates the dependence of the water contact angle of the ozonated and nonozonated SRNOM on pH and calcium content. The measured contact angles for SRNOM were in the 35−46° range indicating that SRNOM is less hydrophobic than Aldrich NOM (α = 74° (*16*)). Both the addition of calcium and ozonation resulted in a decrease in the contact angle of SRNOM in water; the effect of calcium was more pronounced at higher pH values, whereas the effect of ozonation was greater at lower pH values. The same effect of ozonation on the hydrophilicity of NOM was reported by Reckhow and co-workers (*39*). The result is consistent with the fact that the ozonation of the SRNOM produces lower molecular weight, polar, oxygen-rich compounds with a higher content of hydroxyl, carbonylic, and carboxylic groups (*40*). It is not clear, however, why the addition of calcium rendered SRNOM more hydrophilic and why the same trend was not observed when calcium was added to the ozonated SRNOM solution.

The reaction of ozone with the NOM is pH dependent and the predominant mechanisms depend upon pH (i.e., reactions involving molecular O_3 predominate at lower pH and those involving OH radicals and other secondary oxidants predominate at higher pH) (*41*). The chemical nature of the ozonated NOM will depend upon the reaction pH. As a result, the interpretation of the contact angle data for ozonated SRNOM is difficult. For example, SRNOM oxidation by molecular ozone should generate more hydrophilic NOM species than those produced during the oxidation of NOM by ·OH. This difference, however, is countered by the protonation of hydrophilic functional groups at lower pH.

3.3. Free Energy of SRNOM−SRNOM Cohesion and SRNOM-TiO_2 Adhesion. The hydrophilicity of the SRNOM determines the magnitude of the forces of hydrophilic repulsion or hydrophobic attraction (i.e., acid−base forces) that, together with electrostatic and van der Waals forces, define SRNOM interactions with other SRNOM colloids and with the TiO_2 nanoparticles. To quantitatively evaluate acid−base interactions, contact angle measurements with two more probe liquids with known surface tension parameters were conducted. Based on measured contact angles and estimated surface tension parameters (see SI Table SI1), free energies of adhesion (eqs 1−3) corresponding to electrostatic, van der Waals, and acid−base forces were calculated for the cases of adhesion of (1) ozonated and (2) nonozonated SRNOM to the surface of a TiO_2 nanoparticle at different pH values (Figure 2).

Short range NOM−NOM and NOM−TiO_2 interactions were governed by polar (acid−base) and van der Waals forces, while the contribution of electrostatic interaction ($\Delta G_{y_0}^{EL}$) was found to be minor (see SI Figures SI3 and SI4). The most salient trend in the interaction energy was the effect of ozonation at pH 3 and pH 5, which, in the absence of calcium, increased the relative contribution of hydrophilic repulsion between SRNOM molecules and between SRNOM and TiO_2. Dramatic changes were observed in the electron donor and electron acceptor components of free energy of the SRNOM interactions. Ozonation led to an increase in the value of the electron donor component of free energy (γ^-), resulting in more positive values of the acid−base interaction energy

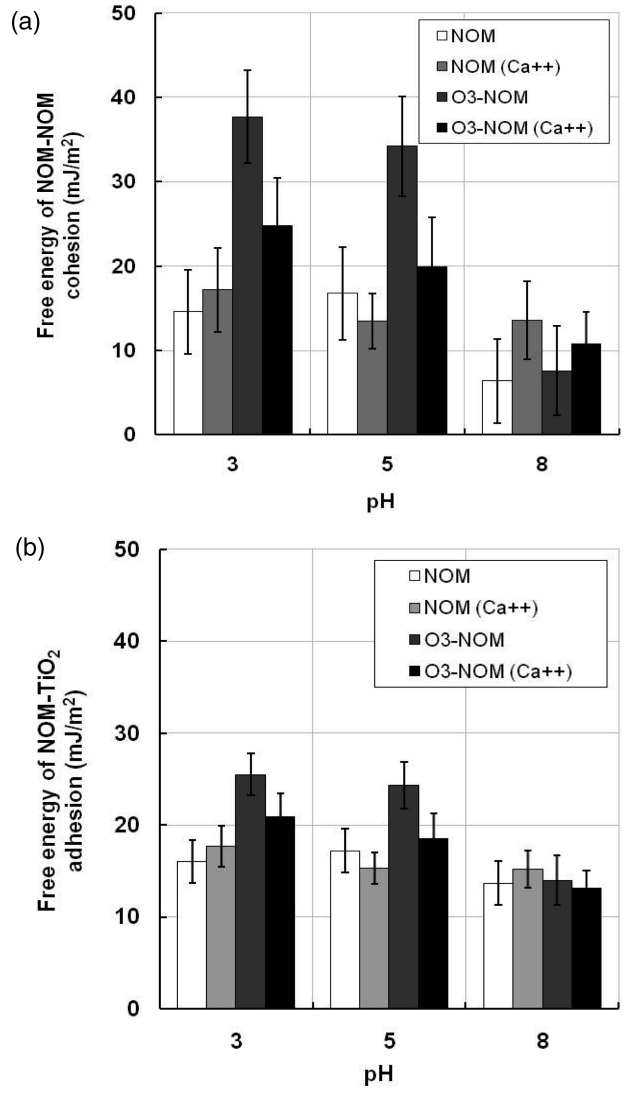

FIGURE 2. Combined effect of pH, Ca^{2+}, and preozonation on the XDLVO energy of interaction between (a) SRNOM molecules, and (b) SRNOM molecule and TiO_2 surface. The error bars correspond to 90% confidence intervals.

($\Delta G_{y_0}^{AB}$). This increase, reflected by the increase in hydrophilicity determined in contact angle measurements, was more pronounced at lower pH.

The addition of calcium decreased the differences in interaction energies for both ozonated and nonozonated SRNOM. In view of the observed strong effect of calcium on adsorption (Figure 3) and permeate flux (Figure 4), this observation indicates that non-XDLVO forces (e.g., steric effects, bridging by calcium) may play an important role in SRNOM−SRNOM and SRNOM−TiO_2 interactions.

The trends observed for the free energy of the SRNOM-TiO_2 adhesion as a function of ozonation, pH and calcium content (SI Table SI2, upper half) were qualitatively the same as those for the energy of cohesive interaction of a pair of SRNOM molecules implying that the short-range SRNOM-TiO_2 interaction energy are governed by the properties of the SRNOM molecules and not the properties of the TiO_2 surface. It follows that the SRNOM sorption onto TiO_2 is insensitive to the amount of SRNOM already sorbed on the TiO_2 surface.

3.4. Adsorption Isotherms. The adsorption kinetics experiments (SI Figure SI5) showed that at pH 3 the equilibrium between the dissolved and adsorbed SRNOM phases was reached after ca. 10 h. Based on these results a

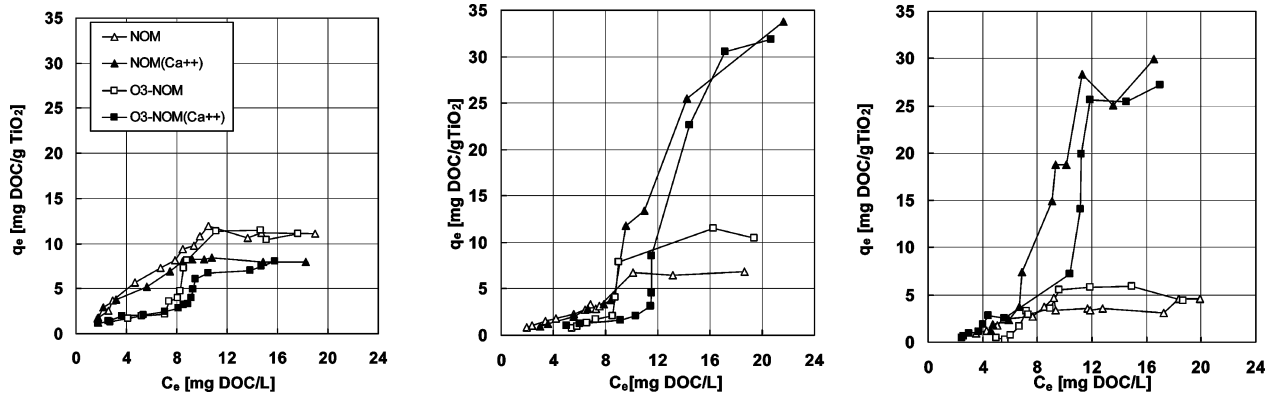

FIGURE 3. Isotherm of adsorption of ozonated and nonozonated SRNOM onto the surface of TiO_2 nanoparticles at pH 3 (left), pH 5 (center), and pH 8 (right).

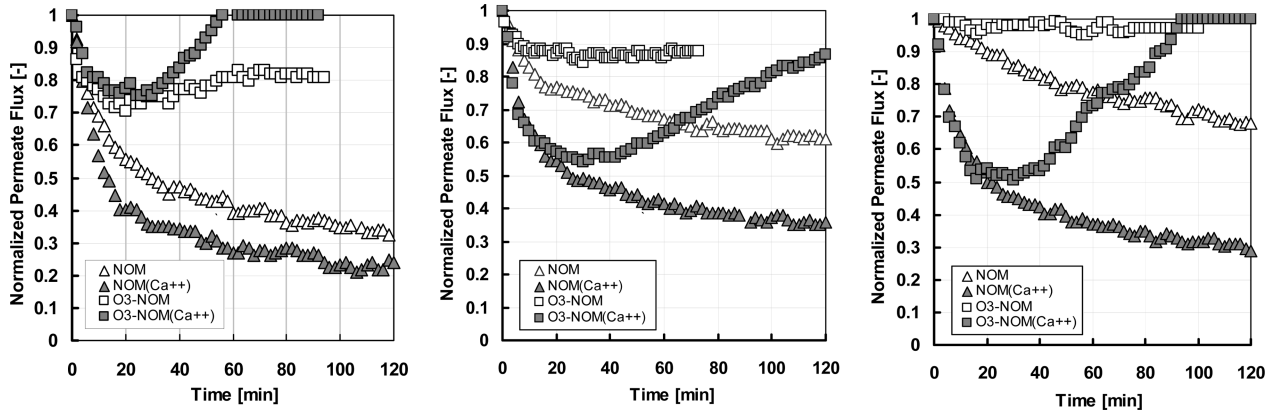

FIGURE 4. Combined effect of pH and Ca^{2+} on flux decline in a hybrid ozonation−ceramic membrane filtration system: pH 3 (left), pH 5 (center), and pH 8 (right).

contact time of 24 h was chosen for all isotherm measurements. Figure 3 presents the adsorption isotherms for ozonated and nonozonated SRNOM by the TiO_2 nanoparticles, both in the presence and absence of calcium. The ozonation of the SRNOM solution and the availability of Ca^{2+} both affected adsorption behavior.

Depending on the pH and TiO_2 loading, the adsorption of SRNOM species was found to be affected by either the availability of the divalent cations or by the ozonation of SRNOM. For higher TiO_2 loadings (i.e., lower values of equilibrium liquid phase concentration of SRNOM, $C_e < 6$ mg/L) at pH 3 and pH 5, the isotherms of the nonozonated SRNOM differed markedly from the isotherms of ozonated SRNOM regardless of the calcium content of the solution. The salient feature of this regime was that ozonation resulted in decreased adsorption, as manifested by lower values of the equilibrium adsorbent-phase concentration, q_e^{max}. The decreased adsorption of the ozonated SRNOM can be explained by its more hydrophilic nature. For the ozonated SRNOM, the adsorption isotherms have a concave shape suggesting that adsorption is unfavorable under these conditions.

For lower TiO_2 loadings, the adsorption at pH 5 and pH 8 was strongly affected by the presence of calcium. Adsorption was significantly greater than that observed at pH 3 (Figure 3a). Specifically, at pH 3 the equilibrium loading, q_e^{max}, of SRNOM on TiO_2 surface was 8 mg(DOC)/g(TiO_2), whereas for higher pH values q_e^{max} was in the (27 to 34) mg(DOC)/g(TiO_2) range. At pH 5 and pH 8, the presence of calcium resulted in an increase in q_e^{max}, at pH 3 calcium had little effect on q_e^{max} (-▲- and -■- versus -□- and -Δ-, Figure 3a). The effect of the addition of Ca^{2+} cannot be explained solely in terms of the XDLVO interactions between SRNOM−SRNOM and SRNOM−TiO_2 interactions. This indicates that non-XDLVO interactions, such as steric effects and/or SRNOM bridging by calcium, are important in this system. Specifically, the observed adsorption behavior in the calcium-controlled regime can be rationalized in terms of SRNOM−TiO_2 and/or SRNOM−SRNOM bridging by calcium. At high pH, the SRNOM and TiO_2 nanoparticles have a strong negative charge (Figure 1a) favoring SRNOM−SRNOM intermolecular bridging, potentially resulting in a multilayer sorption, which can explain the enhancement in the amount of sorbed SRNOM (*21, 42*−*44*).

In the absence of calcium, the amount of sorbed SRNOM decreases with pH (Figure 3, -▲- and -Δ-). This is consistent with the fact that SRNOM adopts a more compact conformation at lower pH (*45*) and can pack more densely at the TiO_2 surface. At pH 3, in the case of lower TiO_2 loadings ($C_e \geq 16$ mg/L), adsorption is again affected by the availability of Ca^{2+} (Figure 3a). In the absence of Ca^{2+}, maximum solid phase concentration q_e^{max} was ca. 12 mg(DOC)/g(TiO_2) for both ozonated and nonozonated SRNOM. The value of q_e^{max} was ca. 1.5 times higher than that for the adsorption of these species when Ca^{2+} was present.

The implications of the above results extend beyond the mitigation of membrane fouling and disinfection byproduct formation. Nanoscale TiO_2 is manufactured and used in household products at increasingly large scale. Understanding TiO_2−NOM interactions is important for predicting the transport and fate of TiO_2 nanoparticles in natural waters and water treatment systems.

3.5. Permeate Flux Performance of the Hybrid Membrane Filtration-Ozonation System. The transient behavior of the permeate flux in the hybrid filtration−ozonation system is shown in Figure 4. Retentate crossflow rate, ozone gas flow rate, and transmembrane pressure were kept the same in all filtration experiments. The initial decrease in

the permeate flux can be attributed to the initial ozone demand that needs to be met before a noticeable degradation of the NOM fouling layer can take place. Once the ozone demand is met, the ozonation of the cake-forming NOM results in the decrease of the cake's hydraulic resistance to the extent that the change translates into an observable increase of the permeate flux. The rate of flux recovery is a complex function of the accessibility of (1) NOM deposited onto the membrane surface and (2) the catalytic membrane surface to ozone and secondary radical species (*12*).

For the nonozonated SRNOM in the absence of calcium, there was a clear correlation between pseudo steady state values of the normalized permeate flux (-Δ-, Figure 4) and the maximum amount of NOM in the adsorbed phase (-Δ-, Figure 3): $J_{ss} \approx 0.3$, 0.6, 0.7, and $q_{max} \approx 12$, 7, 5 (mg(DOC)/g(TiO_2)) for pH 3, 5, 8, respectively. At pH 5 and pH 8, the addition of calcium resulted in a more rapid permeate flux decline (-▲-, Figure 4b and c), which corresponds to significantly higher q_{max} values observed under these conditions (-▲-, Figure 3b and c). The relatively small Ca^{2+}-induced decrease in q_{max} at pH 3 (-▲-, Figure 3a), however, did not result in a decrease in fouling (-▲-, Figure 4a). Ozonation, as anticipated, improved flux performance for all combinations of pH and Ca^{2+} concentrations (-□- and -■-, Figure 4). At pH 8, the relatively small amount of sorbed SRNOM (-Δ-, Figure 3c), could be completely and continuously removed by ozone injection (-▲-, Figure 4c) and the flux was restored to its initial value ($J_{ss} \approx 1$). Again, a correlation between the effect of Ca^{2+} addition on ozonated SRNOM adsorption and flux performance was observed. The Ca^{2+}-induced decrease in sorbed ozonated SRNOM at pH 3 (-□- vs -■-, Figure 3) corresponded to higher permeate fluxes (-□- vs -■-, Figure 4) while more sorption, in the presence of Ca^{2+}, at pH 5 and pH 8 led to lower fluxes at these pH values.

Several factors made the conditions in the adsorption batch reactor and in the hybrid filtration−ozonation reactor dissimilar: (i) the bleeding of the retentate, (ii) the continuous injection of ozone gas into the retentate line in the hybrid system, (iii) the duration of filtration experiments (less than 2 h), which was significantly shorter than the time necessary to achieve adsorption equilibrium (see SI), (iv) changes to the TiO_2 nanoparticles caused by sintering at time of membrane. Despite these differences, however, the adsorption data proved to be predictive of the permeate flux performance.

Acknowledgments

This work was supported by the National Science Foundation research grants CBET-056828 and OISE-0530174. The authors thank Dr. Merlin Bruening (Department of Chemistry, MSU) for providing access to the FTA 200 analyzer.

Note Added after ASAP Publication

Due to a production error, Figure 4 caption was modified in the version of this paper published ASAP June 16, 2009; the corrected version published ASAP June 17, 2009.

Supporting Information Available

Additional data on the hybrid ozonation-ultrafiltration unit, characterization of TiO_2 nanoparticle charge, contact angle measurements, details of XDLVO modeling results, and effects of pH on the concentrations of NOM and dissolved ozone in the retentate.This material is available free of charge via the Internet at http://pubs.acs.org.

Literature Cited

(1) Kwak, S. Y.; Kim, S. H.; Kim, S. S. Hybrid organic/inorganic reverse osmosis (RO) membrane for bactericidal anti-fouling. 1. Preparation and characterization of TiO_2 nanoparticle self-assembled aromatic polyamide thin-film-composite (TFC) membrane. *Environ. Sci. Technol.* **2001**, *35*, 2388–2394.

(2) Molinari, R.; Palmisano, L.; Drioli, E.; Schiavello, M. Studies on various reactor configurations for coupling photocatalysis and membrane processes in water purification. *J. Membr. Sci.* **2002**, *206*, 399–415.

(3) Kim, S. H.; Kwak, S. Y.; Sohn, B. H.; Park, T. H. Design of TiO2 nanoparticle self-assembled aromatic polyamide thin-film-composite (TFC) membrane as an approach to solve biofouling problem. *J. Membr. Sci.* **2003**, *211*, 157–165.

(4) Bae, T. H.; Kim, I. C.; Tak, T. M. Preparation and characterization of fouling-resistant TiO2 self-assembled nanocomposite membranes. *J. Membr. Sci.* **2006**, *275*, 1–5.

(5) Karnik, B. S.; Davies, S. H.; Chen, K. C.; Jalowski, D. R.; Baumann, M. J.; Masten, S. J. Effect of ozonation on the permeate flux of nanocrystalline ceramic membranes. *Water Res.* **2005**, *39*, 728–734.

(6) Karnik, B. S.; Davies, S. H.; Baumann, M. J.; Masten, S. J. Fabrication of catalytic membranes for the treatment of drinking water using combined ozonation and ultrafiltration. *Environ. Sci. Technol.* **2005**, *39*, 7656–7661.

(7) Karnik, B. S.; Davies, S. H.; Chen, K. C.; Jaglowski, D. R. B., M. J.; Masten, S. J. Effects of ozonation on the permeate flux of nanocrystalline ceramic membranes. *Water Res.* **2005**, *39*, 728–734.

(8) Karnik, B. S.; Davies, S. H.; Baumann, M. J.; Masten, S. J. The effects of combined ozonation and filtration on disinfection by-product formation. *Water Res.* **2005**, *39*, 2839–2850.

(9) Choi, H.; Stathatos, E.; Dionysiou, D. D. Sol-gel preparation of mesoporous photocatalytic TiO_2 films and TiO_2/Al_2O_3 composite membranes for environmental applications. *Appl. Catal., B* **2006**, *63*, 60–67.

(10) Karnik, B. S.; Davies, S. H.; Baumann, M. J.; Masten, S. J. Use of salicylic acid as a model compound to investigate hydroxyl radical reaction in ozonation-membrane filtration hybrid process. *Environ. Eng. Sci.* **2007**, *24*, 852–860.

(11) Huang, X. H.; Leal, M.; Li, Q. L. Degradation of natural organic matter by TiO_2 photocatalytic oxidation and its effect on fouling of low-pressure membranes. *Water Res.* **2008**, *42*, 1142–1150.

(12) Kim, J.; Davies, S. H.; Baumann, M. J.; Tarabara, V. V.; Masten, S. J. Effect of ozone dosage and hydrodynamic conditions on the permeate flux in a hybrid ozonation-ceramic ultrafiltration system treating natural waters. *J. Membr. Sci.* **2008**, *311*, 165–171.

(13) Jucker, C.; Clark, M. M. Adsorption of aquatic humic substances on hydrophobic ultrafiltration membranes. *J. Membr. Sci.* **1994**, *97*, 37–52.

(14) Howe, K. J.; Clark, M. M. Fouling of microfiltration and ultrafiltration membranes by natural waters. *Environ. Sci. Technol.* **2002**, *36*, 3571–3576.

(15) Cho, J.; Amy, G.; Pellegrino, J.; Yoon, Y. Characterization of clean and natural organic matter (NOM) fouled NF and UF membranes, and foulants characterization. *Desalination* **1998**, *118*, 101–108.

(16) Yuan, W.; Zydney, A. L. Humic acid fouling during ultrafiltration. *Environ. Sci. Technol.* **2000**, *34*, 5043–5050.

(17) Violleau, D.; Essis-Tome, H.; Habarou, H.; Croué, J. P.; Pontié, M. Fouling studies of a polyamide nanofiltration membrane by selected natural organic matter: an analytical approach. *Desalination* **2005**, *173*, 223–238.

(18) Childress, A. E.; Elimelech, M. Effect of solution chemistry on the surface charge of polymeric reverse osmosis and nanofiltration membranes. *J. Membr. Sci.* **1996**, *119*, 253–268.

(19) Braghetta, A.; DiGiano, F. A.; Ball, W. P. Nanofiltration of natural organic matter: pH and ionic strength effects. *J. Environ. Eng.-ASCE* **1997**, *123*, 628–641.

(20) Hong, S.; Elimelech, M. Chemical and physical aspects of natural organic matter (NOM) fouling of nanofiltration membranes. *J. Membr. Sci.* **1997**, *132*, 159–181.

(21) Li, Q.; Elimelech, M. Organic fouling and chemical cleaning of nanofiltration membranes: Measurements and mechanisms. *Environ. Sci. Technol.* **2004**, *38*, 4683–4693.

(22) Nazzal, F. F.; Wiesner, M. R. pH and ionic strength effects on the performance of ceramic membranes in water filtration. *J. Membr. Sci.* **1994**, *93*, 91–103.

(23) Schlichter, B.; Mavrov, V.; Chmiel, H. Study of a hybrid process combining ozonation and microfiltration/ultrafiltration for drinking water production from surface water. *Desalination* **2004**, *168*, 307–317.

(24) Lee, S.; Lee, K.; Wan, W. M.; Choi, Y. Comparison of membrane permeability and a fouling mechanism by pre-ozonation followed by membrane filtration and residual ozone in membrane cells. *Desalination* **2005**, *178*, 287–294.

(25) von Gunten, U. Ozonation of drinking water: Part I. Oxidation kinetics and product formation. *Water Res.* **2003**, *37*, 1443–1467.
(26) Stumm, W.; Morgan, J. J. *Aquatic chemistry: Chemical equilibria and rates in natural waters*, 3rd ed.; John Wiley & Sons, Inc.: New York, 1996.
(27) Derjaguin, B. V.; Landau, L. D. Theory of the stability of strongly charged lyophobic sols and of the adhesion of strongly charged particles in solutions of electrolytes. *Acta Physiochim. URSS* **1941**, *14*, 633–662.
(28) Verwey, E. J. W.; Overbeek, J. T. G. Theory of the stability of lyophobic colloids. In *The interaction of particles having an electric double layer*; Elsevier: Amsterdam, 1948.
(29) Van Oss, C. J. Acid-base interfacial interactions in aqueous media. *Colloid Surf., A* **1993**, *78*, 1–49.
(30) Brant, J. A.; Childress, A. E. Assessing short-range membrane-colloid interactions using surface energetics. *J. Membr. Sci.* **2002**, *203*, 257–273.
(31) Kang, S.-T.; Subramani, A.; Hoek, E. M. V.; Deshusses, A.; Matsumoto, M. R. Direct observation of biofouling in cross-flow microfiltration: mechanisms of deposition and release. *J. Membr. Sci.* **2004**, *244*, 151–165.
(32) Kim, S.; Marion, M.; Jeong, B.-H.; Hoek, E. M. V. Crossflow membrane filtration of interacting nanoparticle suspensions. *J. Membr. Sci.* **2006**, *284*, 361–372.
(33) Van Oss, C. J. *Interfacial Forces in Aqueous Media*, 2nd ed.; Taylor & Francis: Boca Raton, FL, 2006.
(34) Hoek, E. M. V.; Agarwal, G. K. Extended DLVO interactions between spherical particles and rough surfaces. *J. Colloid Interface Sci.* **2006**, *298*, 50–58.
(35) Chusuei, C. C.; Goodman, D. W.; Van Stipdonk, M. J.; Justes, D. R.; Loh, K. H.; Schweikert, E. A. Solid-liquid adsorption of calcium phosphate on TiO_2. *Langmuir* **1999**, *15*, 7355–7360.
(36) Chandrakanth, M. S.; Amy, G. L. Effects of NOM source variations and calcium complexation capacity on ozone-induced particle destabilization. *Water Res.* **1998**, *32*, 115–124.
(37) Cornel, P. K.; Summers, R. S.; Roberts, P. V. Diffusion of humic-acid in dilute aqueous-solution. *J. Colloid Interface Sci.* **1986**, *110*, 149–164.
(38) Chandrakanth, M. S.; Amy, G. L. Effects of ozone on the colloidal stability and aggregation of particles coated with natural organic matter. *Environ. Sci. Technol.* **1996**, *30*, 431–443.
(39) Bose, P.; Bezbarua, B. K.; Reckhow, D. A. Effect of ozonation on some physical and chemical-properties of aquatic natural organic-matter. *Ozone: Sci. Eng.* **1994**, *16*, 89–112.
(40) Moon, J.; Kim, S. H.; Cho, J. Characterizations of natural organic matter as nano particle using flow field-flow fractionation. *Colloid Surf., A* **2006**, *287*, 232–236.
(41) Langlais, B.; Reckhow, D. A.; Brink, D. R. *Ozone in water treatment: Application and engineering: Cooperative research report*; Lewis Publishers: Chelsea, Mich., 1991.
(42) Lofts, S.; Tipping, E. An assemblage model for cation binding by natural particulate matter. *Geochim. Cosmochim. Acta* **1998**, *62*, 2609–2625.
(43) Tsuru, T.; Hironaka, D.; Yoshioka, T.; Asaeda, M. Effect of divalent cations on permeate volume through porous titania membrane. *Desalination* **2002**, *147*, 213–216.
(44) Ahn, W.-Y.; Kalinichev, A. G.; Clark, M. M. Effects of background cations on the fouling of polyethersulfone membranes by natural organic matter: experimental and molecular modeling study. *J. Membr. Sci.* **2008**, *309*, 128–140.
(45) Ghosh, K.; Schnitzer, M. Macromolecular structures of humic substances. *Soil Sci.* **1980**, *129*, 266–276.

ES900342Q